

Fulde-Ferrell-Larkin-Ovchinnikov Phases in Two-dimensional Spin-Orbit Coupled Degenerate Fermi Gases

Zhen Zheng¹, Ming Gong^{2,*}, Yichao Zhang¹, Xubo Zou^{1,†}, Chuanwei Zhang^{2,‡} and Guangcan Guo¹

¹*Key Laboratory of Quantum Information, University of Science and Technology of China, Hefei, Anhui, 230026, People's Republic of China*

²*Department of Physics, The University of Texas at Dallas, Richardson, TX, 75080 USA*

The Fulde-Ferrell-Larkin-Ovchinnikov (FFLO) phase, a superconducting state with non-zero total momentum Cooper pairs in a strong magnetic field, was predicted more than 50 years ago and now becomes an important concept in many branches of physics. However, no unambiguous experimental evidences for the existence of FFLO phases have been observed yet. Recently, spin-imbalanced ultracold degenerate Fermi gases have emerged as a new powerful platform for the observation of FFLO phases due to their high experimental controllability and the lack of disorder. However, in three dimensional degenerate Fermi gases where the FFLO phases can be described within the simple mean field theory, the parameter region for the FFLO phases is too small to be observed in experiments. Recently, we showed that the Rashba type spin-orbit coupling and in-plane Zeeman field in three dimensional degenerate Fermi gases provide a more efficient way to create the FFLO phase because (1) the parameter region for the FFLO phase is greatly enlarged in the phase diagram and (2) the FFLO phase is stabilized due to the enhanced energy difference between FFLO phase and conventional Bardeen-Cooper-Schrieffer (BCS) phase. In this work we investigate the FFLO phase in two dimensional spin-orbit coupled degenerate Fermi gases using the mean field theory, with special concerns on the physical origin of the FFLO state. The basic properties of the FFLO phase are discussed and the phase diagram is obtained at zero temperature. The symmetry of different quantum phases is examined, which provide important basis for the experimental observation of FFLO phases using the time-of-flight imaging.

PACS numbers: 05.30.Fk, 74.20.Fg, 74.25.Dw

I. INTRODUCTION

In 1964, just shortly after the great success of Bardeen-Cooper-Schrieffer (BCS) theory for superconductivity¹, Fulde and Ferrell², and Larkin and Ovchinnikov^{3,4} (FFLO) independently demonstrated that a new type of superconducting state, which is characterized by Cooper pairs with nonzero total momentum and spatially modulated order parameter, may exist in certain regime of a clean superconductor under a strong magnetic field. The superconducting state is now known as the FFLO state. For the BCS cooper pair¹, the pairing takes place between electrons with opposite momentum and spin, i.e., $\mathbf{k} \uparrow$ and $-\mathbf{k} \downarrow$. Therefore when the magnetic field exceeds certain critical value, the superconductivity is destroyed due to Pauli paramagnetic depairing effect. As a consequence, the magnetism and superconductivity generally cannot coexist for the BCS type superconductor, which also fail to explain the origin of magnetic superconductors. The story is totally different for the FFLO phase because these two different orders naturally coexist, or more precisely, the FFLO phase arises from the interplay between magnetism and superconductivity. This important feature makes the FFLO phase a central concept for understanding many exotic phenomena in different physics branches, ranging from unconventional solid state superconductors (e.g., layered^{5,6}, heavy-fermion⁷⁻⁹, organic^{10,11} superconductors, *etc.*), to chiral quark matter in quantum chromodynamics, and to neutron star glitches in astrophysics^{12,13}. In the past several decades,

great efforts have been made to unveil this novel quantum phase, and a lot of exotic signatures that may be related to the FFLO phase have been observed. However, until now, the unambiguous experimental evidences for the existence of FFLO phases are still lacking^{12,14}. There are several reasons for that: firstly, the existence of FFLO phase requires very stringent conditions; and secondly, the direct probing of periodic oscillation of the order parameter is challenging; and thirdly, the disorder effects in the superconductor induce strong scattering between different momenta that destroys the superconducting pairing^{15,16}.

The experimental advances of population imbalanced ultracold Fermi gases have the potential to elucidate this long sought problem. The ultracold atomic system possesses some remarkable advantages over the counterpart in solid state systems due to its high controllability and tunability¹⁷⁻¹⁹. This new platform in principle can be made disorder free, and the disorder, if necessary, can be introduced to the system in a controllable manner²⁰⁻²². On the experimental side, the superfluidity of the Fermi gas can be characterized by the generation of vortices when the gas is rotated²³, and the momentum of the Cooper pair in the FFLO phase can be directly probed using the time-of-flight imaging^{24,25}, while in solid state the direct observation of the FFLO phase is challenging. The main problem is that the FFLO phase only exists in an extremely narrow parameter regime in three dimensional degenerate Fermi gases^{24,26}, therefore in experiments the FFLO phase is generally missed out. For

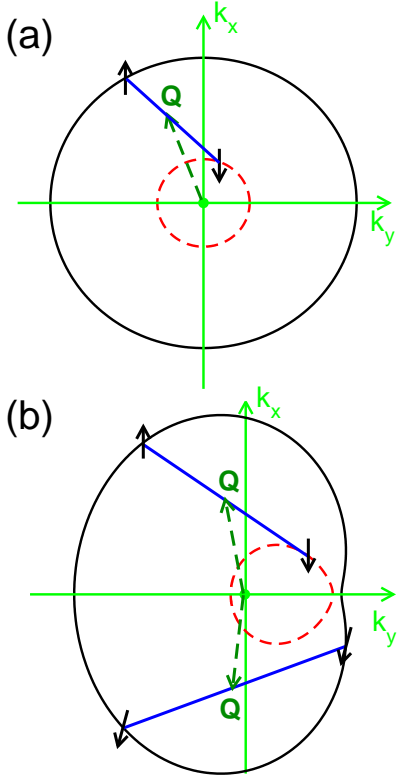


FIG. 1: (Color online) Basic physical picture for the emergence of FFLO phase in ultracold atomic system. (a) shows the creation of FFLO phase with Zeeman field, which is equivalent to the physics by controlling the population imbalance. The mismatched Fermi surface makes the pairing with opposite momentum and spin challenging, thus in some parameter regime the FFLO phase becomes energetically favorable. This mechanism is inefficient because the Pauli paramagnetic depairing effect under strong Zeeman field destroys the Cooper pairs, thus the FFLO phase only survives in a very narrow parameter regime. (b) shows a new mechanism for the generation of FFLO phase using the deformation of the Fermi surface. Such deformation of the Fermi surface can be constructed by an in-plane Zeeman field and SO coupling. The center of the Fermi surface is also shifted due to the Zeeman field, and as a consequence, the BCS type of pairing always becomes challenging even with a small Zeeman field. A very large FFLO phase can be found in the parameter space. The deformation of the Fermi surface breaks the rotational symmetry of the system, thus has the potential to create the FFLO phase with a unique FFLO momentum \mathbf{Q} .

instance, in recent experiments with population imbalanced Fermi gases by Zwierlein *et al*^{27,28} only the phase transition from BCS superfluid to normal gas has been observed, while in another parallel experiment by Partridge *et al*²⁹ the phase separation phase, which is also known as the breached pair³⁰, has been observed. There are two basic reasons why the FFLO phase is missed out in these experiments. Firstly, the parameter space for the FFLO phase is extremely narrow; and secondly, the energy difference between the FFLO ground state and

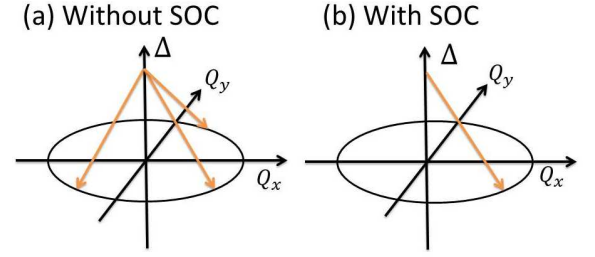


FIG. 2: (Color online) Influence of SO coupling on the emergence of FFLO phase. In (a), the FFLO phase emerges when the Zeeman field exceeds certain critical value. However, the FFLO ground state energy only depends on the magnitude of the FFLO momentum \mathbf{Q} but is independent of the direction, thus in principle all the momenta with the same magnitude ($|\mathbf{Q}| = \text{const}$, see the circle in (a)) are the system's ground state. In the SO coupled system \mathbf{Q} becomes unique in (b) because the SO coupling and in-plane Zeeman field break the rotational symmetry of the model.

BCS excited state is much smaller than the temperature. Therefore even the parameters for the FFLO state have been reached, the FFLO ground state cannot be observed.

In this paper, we show that the above two limitations can be overcome using spin-orbit (SO) coupled degenerate Fermi gases with an in-plane Zeeman field. Different from SO coupling in solid state systems which arises from spatial inversion symmetry breaking³¹, SO coupling in ultracold atoms is generated through laser couplings^{32–37} between hyperfine states, therefore different types of SO coupling can in principle be created by carefully choosing different laser configurations. Experimentally, certain type of SO coupling has been realized using Raman coupling between hyperfine states for both Bose and Fermi gases^{38–43}. In this paper we use Rashba type of SO coupling as an example to demonstrate our basic ideas. The Zeeman field is assumed to be along the x direction, which is in the SO coupling plane. The basic idea for the emergence of the FFLO phase is illustrated in Fig. 1b, which also applies to other types of SO coupling. For the Fermi gas with only Zeeman field, see Fig. 1a, the two mismatched Fermi surfaces always form concentric circles, therefore for the s -wave pairing, the up- and down-spins acquire different Fermi momentum, *i.e.*, $\mathbf{k} + \mathbf{Q}/2, \uparrow$ and $-\mathbf{k} + \mathbf{Q}/2, \downarrow$, with \uparrow and \downarrow spins in the pseudospin representation and \mathbf{Q} as the total momentum of the Cooper pairs. The free energy of the system satisfies the rotational symmetry

$$F(\mathbf{Q}) = F(|\mathbf{Q}|). \quad (1)$$

This is because the Zeeman field only fixes the direction of the spin, but does not fix the direction of the momentum axis, therefore the free energy should have the rotation symmetry for the momentum. It can also be understood from the fact that the total free energy depends on \mathbf{k}^2 , \mathbf{Q}^2 and $\mathbf{k} \cdot \mathbf{Q}$, thus the summation over \mathbf{k} should

be independent of the direction of \mathbf{Q} , see Ref. 24. Physically, Eq. (1) means that the total momentum of the Cooper pair can take any direction therefore the ground state FFLO phase is infinity-fold degenerate. Generally in the numerical simulation, we artificially set \mathbf{Q} along a particular direction and demonstrate that the FFLO phase indeed has a lower energy than the regular BCS superfluid ($\mathbf{Q} = 0$). Due to the Pauli paramagnetic depairing effect, the FFLO phase only survives in a very narrow parameter regime, see also the numerical results in Fig. 4a.

The physical picture is totally different when a Rashba SO coupling is included, as schematically shown in Fig. 1b. In this case the Fermi surface is deformed and the center of the Fermi surface is no longer located at $\mathbf{k} = 0$. Notice that the deformation of the Fermi surface depends strongly on the direction of the SO coupling and Zeeman field. For the model we consider here, the deformation is along the y direction. In the pseudospin representation (the eigenstates of single particle Hamiltonian), we have both singlet pairing and triplet pairing. The triplet pairing is almost intact by the Zeeman field, thus the FFLO phase can be observed in a much larger parameter regime. The deformation of the Fermi surface makes the FFLO phase always energetically favorable even with a small Zeeman field. We have numerically confirmed that the FFLO momentum \mathbf{Q} should be along the y direction, and the minimization of the total free energy should give a single \mathbf{Q} value, therefore the FFLO ground state should be unique, see also Fig. 2b for the movement of \mathbf{Q} in the $\mathbf{Q}-\Delta$ space. For the symmetry argument, see Appendix A.

Generally, the mismatch of the Fermi surface is the basic route to the FFLO phase, and such mismatched Fermi surface can be created by population imbalance²⁷⁻²⁹, Zeeman field²⁶ or mass imbalance^{44,45}. In this work, together with our previous work⁴⁶, we demonstrate that the FFLO phase can be created more efficiently through the deformation of the Fermi surface, which can be constructed by SO coupling, or, non-Abelian gauge field^{32-37,47}, and Zeeman field. Notice that the generation of non-Abelian gauge fields is a subject of intensive investigations in ultracold atoms in the past decade, see a recent review in Ref. 47. For this new route, the Zeeman field is still needed, otherwise, the system has time-reversal symmetry and the band structure should satisfy $E_{\mathbf{k}\uparrow} = E_{-\mathbf{k},\downarrow}$, which means that two atoms with opposite momentum and spin on the Fermi surface can always form BCS Cooper pairs efficiently, leading to BCS superfluid, instead of FFLO phases. Our route here, however, shows that the FFLO phase may become energetically favorable with a small Zeeman field.

In Ref. 46, we have considered a three dimensional degenerate Fermi gas with Rashba SO coupling and an in-plane (in the SO plane) Zeeman field. The FFLO phase cannot be observed in three dimensional solid state systems because the orbital effect is unavoidable no matter which direction the external magnetic field is applied.

The low dimensional systems in solid state materials provide the opportunity for observing FFLO states because the orbital effect can be suppressed by applying a magnetic field parallel to the system, which only leads to a Zeeman field. In ultracold atomic systems, the Zeeman field is generated through different methods without involving the orbital effect, therefore the FFLO state may be observed even in three dimension.

Here we want to emphasize the difference between our proposal and the results in solid state systems⁴⁸. In solid state materials, it has been found that the Rashba type SO coupling in superconducting materials without inversion symmetry can enhance the FFLO phase⁴⁸ by increasing H_{c2} , the so-called upper critical field of the type-II superconductor⁴⁸. In solid state materials, the SO coupling energy αK_F and Zeeman splitting generally are much smaller than E_F , therefore the deformation of the Fermi surface is very small, and cannot be the main driving force for the FFLO phase. In our model the SO coupling energy, Zeeman field and E_F are generally of the same order, thus the deformation of Fermi surface, as shown schematically in Fig. 1b, is significant and provides a major driving force for the formation of the FFLO phase. Moreover, in solid state materials, the disorder effect is one of the major obstacles for the observation of FFLO phase⁴⁹, while the ultracold atomic systems can be made disorder free.

The rest of this work is organized as following. We present our mean field treatment of the SO coupled degenerate Fermi gas with an in-plane Zeeman field in sec. II. Then we plot the phase diagram and discuss its basic properties in sec. III. We discuss the problems related to the measurement of the FFLO phase in sec. IV. At last we conclude in sec. V. The symmetry of the effective Hamiltonian is discussed in Appendix A, and the treatment of the same model using the quantum field theory is presented in Appendix B.

II. PHYSICAL MODEL, HAMILTONIAN, AND GAP EQUATION

We consider a two dimensional degenerate Fermi gas with Rashba-type SO coupling and an in-plane Zeeman field. The two dimensional degenerate Fermi gases can be constructed by applying a strong standing wave along the third direction, and have been realized in recent experiments⁵⁰. The two dimensional SO coupled Fermi gases can be described as

$$H = \sum_{\mathbf{k}\sigma\sigma'} c_{\mathbf{k}\sigma}^\dagger [\xi_{\mathbf{k}\sigma} + \alpha(k_x\sigma_y - k_y\sigma_x) - h\sigma_x] c_{\mathbf{k}\sigma'} + V_{\text{int}}, \quad (2)$$

where α is the SO coupling strength, σ_x and σ_y are the Pauli operators, $\xi_{\mathbf{k}\sigma} = \frac{k^2}{2m} - \mu$, and $\mathbf{k} = (k_x, k_y)$. The last term corresponds to the s -wave scattering interaction

$$V_{\text{int}} = g \sum_{\mathbf{p}_1+\mathbf{p}_2=\mathbf{p}_3+\mathbf{p}_4} c_{\mathbf{p}_1,\uparrow}^\dagger c_{\mathbf{p}_2,\downarrow}^\dagger c_{\mathbf{p}_3,\downarrow} c_{\mathbf{p}_4,\uparrow}, \quad (3)$$

where $\mathbf{p}_1 + \mathbf{p}_2 = \mathbf{p}_3 + \mathbf{p}_4$ due to the conservation of the total momentum during the scattering process, g is the scattering interaction strength.

When atoms form Cooper pairs with a finite total momentum \mathbf{Q} , the scattering process in Eq. 3 can be simplified with $\mathbf{p}_1 = \mathbf{k} + \mathbf{Q}/2$, $\mathbf{p}_2 = -\mathbf{k} + \mathbf{Q}/2$, $\mathbf{p}_3 = \mathbf{p} + \mathbf{Q}/2$, and $\mathbf{p}_4 = -\mathbf{p} + \mathbf{Q}/2$. When $\mathbf{Q} = 0$, the Cooper pairs are formed between two atoms with opposite momentum and spin, recovering the conventional BCS type of pairing. Denote $\beta_{\mathbf{p}} = g c_{\mathbf{p}+\mathbf{Q}/2,\downarrow} c_{-\mathbf{p}+\mathbf{Q}/2,\uparrow}$, the interaction term can be rewritten as $V_{\text{int}} = g \sum_{\mathbf{k},\mathbf{p}} c_{\mathbf{k}+\mathbf{Q}/2,\uparrow}^\dagger c_{-\mathbf{k}+\mathbf{Q}/2,\downarrow}^\dagger c_{\mathbf{p}+\mathbf{Q}/2,\downarrow} c_{-\mathbf{p}+\mathbf{Q}/2,\uparrow} = \sum_{\mathbf{k},\mathbf{p}} \frac{\beta_{\mathbf{k}}^\dagger \beta_{\mathbf{p}}}{g}$. The interaction term can be decoupled using the standard mean-field method

$$\beta_{\mathbf{k}}^\dagger \beta_{\mathbf{p}} \rightarrow \langle \beta_{\mathbf{k}}^\dagger \rangle \beta_{\mathbf{p}} + \beta_{\mathbf{k}}^\dagger \langle \beta_{\mathbf{p}} \rangle - \langle \beta_{\mathbf{k}}^\dagger \rangle \langle \beta_{\mathbf{p}} \rangle, \quad (4)$$

where the order parameter in the momentum space $\Delta = \sum_{\mathbf{p}} g \langle c_{\mathbf{p}+\mathbf{Q}/2,\downarrow} c_{-\mathbf{p}+\mathbf{Q}/2,\uparrow} \rangle$. The interaction term now reduces to

$$V_{\text{int}} = \sum_{\mathbf{k}} \Delta \beta_{\mathbf{k}}^\dagger + \Delta^* \beta_{\mathbf{k}} - \frac{|\Delta|^2}{g}. \quad (5)$$

Notice that $c_{\mathbf{p}\sigma} = \int d\mathbf{x} c_\sigma(\mathbf{x}) e^{-i\mathbf{p}\cdot\mathbf{x}}$, then we have the pairing in the real space,

$$\begin{aligned} \langle c_\uparrow(\mathbf{x}) c_\downarrow(\mathbf{y}) \rangle &= \int d\mathbf{p} d\mathbf{p}' \langle g c_{\mathbf{p},\uparrow} c_{\mathbf{p}',\downarrow} \rangle e^{i(\mathbf{p}\cdot\mathbf{x} + \mathbf{p}'\cdot\mathbf{y})} \\ &= \Delta \delta(\mathbf{x} - \mathbf{y}) e^{i\mathbf{Q}\cdot\mathbf{x}}. \end{aligned} \quad (6)$$

We see the order parameter defined in the momentum space corresponds to a non-uniform pairing in the real space. The δ -function arises from the contact interaction. The above pairing breaks the time-reversal symmetry, which is in consistent with our model because a Zeeman field is applied.

Using the standard Bogliubov transformation, the Hamiltonian can be rewritten as

$$H = \frac{1}{2} \sum_{\mathbf{k}} \psi_{\mathbf{k},\mathbf{Q}}^\dagger H_{\text{eff}} \psi_{\mathbf{k},\mathbf{Q}} - \frac{|\Delta|^2}{g} + \frac{1}{2} \sum_{\mathbf{k},\sigma} \xi_{\mathbf{k}\sigma}, \quad (7)$$

where the effective Hamiltonian reads as,

$$H_{\text{eff}} = \begin{pmatrix} \mathcal{K}(\mathbf{k}) & \Delta I_{2 \times 2} \\ \Delta^\dagger I_{2 \times 2} & -\sigma_y \mathcal{K}^*(-\mathbf{k}) \sigma_y \end{pmatrix} \quad (8)$$

with

$$\mathcal{K}(\mathbf{k}) = \begin{pmatrix} \xi_{\mathbf{k}+\mathbf{Q}/2,\uparrow} & h - \alpha R(\mathbf{k}) \\ h - \alpha R(\mathbf{k})^* & \xi_{\mathbf{k}+\mathbf{Q}/2,\downarrow} \end{pmatrix}, \quad (9)$$

$R(\mathbf{k}) = (\mathbf{k} + \mathbf{Q}/2)_x + i(\mathbf{k} + \mathbf{Q}/2)_y$ and $I_{2 \times 2} = \text{diag}(1, 1)$. The basis defined in Eq. 7 is $\psi_{\mathbf{k},\mathbf{Q}} = (c_{\mathbf{k}+\mathbf{Q}/2,\uparrow}, c_{\mathbf{k}+\mathbf{Q}/2,\downarrow}, c_{-\mathbf{k}+\mathbf{Q}/2,\downarrow}^\dagger, -c_{-\mathbf{k}+\mathbf{Q}/2,\uparrow}^\dagger)^T$. The minus sign in the last term in the basis is essential to achieve the $\Delta I_{2 \times 2}$ type of off-diagonal term in Eq. 8.

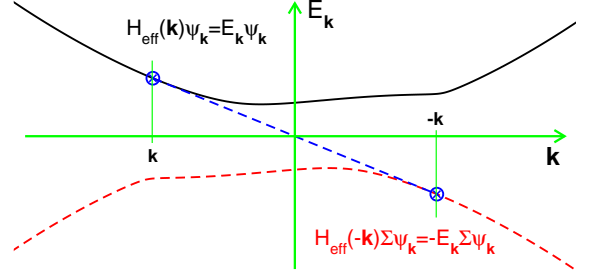


FIG. 3: Particle-hole symmetry in our model. The particle-hole symmetry establishes the direct relation between $\psi_{\mathbf{k}}$ for $H_{\text{eff}}(\mathbf{k})$ with eigenvalues $E_{\mathbf{k}}$ to $\Sigma \psi_{\mathbf{k}}$ for $H_{\text{eff}}(-\mathbf{k})$ with eigenvalues $-E_{\mathbf{k}}$. Due to the lack of chiral symmetry⁵¹, the eigenvalues of $H_{\text{eff}}(\mathbf{k})$ may not appear with pairs. The particle-hole correspondence is shown via dashed line.

The symmetry of the system is essential for understanding the properties of different quantum phases, and directly related to the measurement of the FFLO state using the time-of-flight measurement. We first consider the particle-hole symmetry of the model. The particle-hole operator can be written as $\Sigma = \Lambda K$, where $\Lambda = \sigma_y \tau_y$ (σ_y is the Pauli spin matrix and τ_y is the Nambu particle-hole matrix), and K represents the complex conjugate operator. Λ is a unitary operator, and $\Lambda = \Lambda^{-1}$. K is an antiunitary operator because $K^2 = 1$, which is used to ensure that Σ is an antiunitary operator. Note that the system does not have the time-reversal symmetry but has the particle-hole symmetry with $\Sigma^2 = \Lambda K \Lambda K = \Lambda \Lambda^* = \Lambda^2 = 1$, therefore the system belongs to the symmetry class D , see Ref. 51. We have

$$\begin{aligned} \Sigma H_{\text{eff}}(\mathbf{k}) \Sigma^{-1} &= \Lambda H_{\text{eff}}^*(\mathbf{k}) \Lambda \\ &= \Lambda \begin{pmatrix} \mathcal{K}^*(\mathbf{k}) & \Delta^\dagger I_{2 \times 2} \\ \Delta I_{2 \times 2} & -\sigma_y \mathcal{K}(-\mathbf{k}) \sigma_y \end{pmatrix} \begin{pmatrix} 0 & -i\sigma_y \\ i\sigma_y & 0 \end{pmatrix} \\ &= \begin{pmatrix} 0 & -i\sigma_y \\ i\sigma_y & 0 \end{pmatrix} \begin{pmatrix} i\Delta^\dagger \sigma_y & -i\mathcal{K}^*(\mathbf{k}) \sigma_y \\ -i\sigma_y \mathcal{K}(-\mathbf{k}) & -i\Delta \sigma_y \end{pmatrix} \\ &= \begin{pmatrix} -\mathcal{K}(-\mathbf{k}) & -\Delta I_{2 \times 2} \\ -\Delta^\dagger I_{2 \times 2} & \sigma_y \mathcal{K}^*(\mathbf{k}) \sigma_y \end{pmatrix} \\ &= -H_{\text{eff}}(-\mathbf{k}). \end{aligned} \quad (10)$$

Here Σ establishes a one-to-one correspondence between \mathbf{k} and $-\mathbf{k}$, therefore if $\psi_{\mathbf{k}} = (u(\mathbf{k}), v(\mathbf{k}))^T$ is an eigenvector of the Hamiltonian $H_{\text{eff}}(\mathbf{k})$ with energy $E_{\mathbf{k}}$, then $\psi'_{\mathbf{k}} = \Sigma \psi_{\mathbf{k}} = (\sigma_y v^*(\mathbf{k}), -\sigma_y u^*(\mathbf{k}))^T$ is the eigenvector of the Hamiltonian $H_{\text{eff}}(-\mathbf{k})$ with energy $-E(\mathbf{k})$, as schematically shown in Fig. 3. The particle-hole symmetry does not automatically ensure that the eigenenergies appear in pairs ($E, -E$) because the system lacks the chiral symmetry⁵¹. This is a direct consequence of the rotational symmetry breaking for our model due to the in-plane Zeeman field. However, for an out-of-plane Zeeman field, we observe that all eigenvalues still appear with pairs, see more details in Appendix A. For the BCS superfluid, we find $\text{tr}(H_{\text{eff}}(\mathbf{k})) = \sum_{\lambda} E_{\lambda} = 0$, while for

the FFLO phase, we find $\text{tr}(H_{\text{eff}}(\mathbf{k})) = \frac{2\mathbf{k} \cdot \mathbf{Q}}{m} \neq 0$. Therefore for the FFLO phase, the eigenvalues never appear with pairs no matter which direction the Zeeman field takes.

We are interested in the particular case when \mathbf{Q} is along the y -axis (i.e., $\mathbf{Q}_x = 0$). In this case, the system has a discrete Z_2 symmetry, i.e., the band structure is invariant under transformation $k_x \rightarrow -k_x$, hence $E_\lambda(k_x, k_y) = E_\lambda(-k_x, k_y)$. Such symmetry can be directly probed using the time-of-flight imaging, see below. We also find that a topological phase transition may take place when $h = \sqrt{\mu^2 + \Delta^2}$ for the BCS superfluid, which can be obtained following the same procedure in Ref. 52, see also Appendix A. In our numerical simulation, we find that the Zeeman field and SO coupling generally reduce the order parameter strength, and the superfluid is always destroyed before entering the topological BCS superfluid regime. The topological superfluid may be observed when the out-of-plane and in-plane Zeeman fields are presented simultaneously. However, since the particle and hole may not appear with pairs due to the rotational symmetry breaking, it may not be suitable for the observation the associated topological excitations, such as the zero-energy Majorana Fermion. With only out-of-plane Zeeman field, the topological phase transition has been intensively discussed in the literature recently^{53–59}. The model with in-plane Zeeman field generally favors the FFLO phase and suppresses the topological superfluid, therefore only regular BCS superfluid phase, FFLO phase, and normal gas phase can be observed in our model.

The thermodynamical potential at zero temperature reads as

$$\Omega = -\frac{\Delta^2}{g} + \frac{1}{2} \sum_{\mathbf{k}\sigma} \xi_{\mathbf{k}\sigma} + \frac{1}{2} \sum_{\mathbf{k},\lambda} E_\lambda \Theta(-E_\lambda), \quad (11)$$

where the Heaviside step function

$$\Theta(x) = \begin{cases} 1, & x \geq 0 \\ 0, & x < 0 \end{cases}. \quad (12)$$

E_λ , $\lambda = 1, 2, 3$ and 4 , are the eigenvalues of the effective Hamiltonian H_{eff} , whose exact expressions are too complex to be presented here. To facilitate the further investigation of the FFLO phase, especially the physics at finite temperature where the fluctuation effect becomes important, we also derive the same thermodynamical potential using the quantum field theory, see Appendix B. We therefore see the standard mean-field decoupling used in Eq. 4 actually corresponds to the Hubbard-Stratanovich transformation in the quantum field theory. We use the mean field theory as the main theoretical tool in this work because it provides a more transparent interpretation of the FFLO physics.

The effective scattering interaction g in Eq. 11 in a two dimensional Fermi gas should be regularized using⁶⁰

$$\frac{1}{g} = - \sum_{\mathbf{k}} \frac{1}{\mathbf{k}^2/m + E_b}, \quad (13)$$

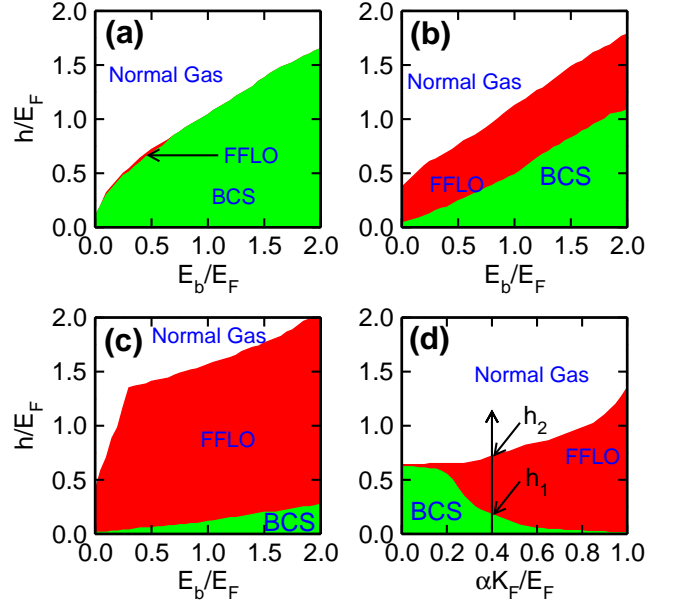


FIG. 4: (Color online). Phase diagram of the two dimensional degenerate Fermi gas in the presence of Rashba-type SO coupling and an in-plane Zeeman field. (a) results with vanishing SO coupling. (b), (c) correspond to the results with SO coupling $\alpha K_F = 0.5$ and $\alpha K_F = 1.0$, respectively. (d) shows the phase diagram in the $h - \alpha K_F$ plane at $E_b = 0.4 E_F$. h_1 (h_2) defines the boundary between BCS (FFLO) and FFLO (normal gas) phase. In our calculation, we do not observe topological superfluid phases.

where the binding energy E_b can be tuned by varying the s -wave scattering length through Feshbach resonance^{17–19}.

The order parameter Δ , chemical potential μ , and the FFLO momentum \mathbf{Q} should be solved self-consistently due to the conservation of atom number, i.e.,

$$\frac{\partial \Omega}{\partial \mu} = -n, \quad \frac{\partial \Omega}{\partial \Delta} = 0, \quad \frac{\partial \Omega}{\partial \mathbf{Q}} = 0. \quad (14)$$

Here Δ and \mathbf{Q} are used to minimize the thermodynamical potential Ω . We consider three different quantum phases: the normal phase with $\Delta = 0$ and $\mathbf{Q} = 0$ (for the normal gas \mathbf{Q} does not enter the effective free energy, thus can be any value. We force $\mathbf{Q} = 0$); The BCS type of superfluid with $\mathbf{Q} = 0$ but $\Delta \neq 0$; and the FFLO phase with $\mathbf{Q} \neq 0$ and $\Delta \neq 0$. When we fix $\mathbf{Q} = 0$ then only BCS type of superfluid phase and the normal gas can be obtained. Throughout this work, we use two different strategies to check the influence of \mathbf{Q} on the formation of the FFLO phase. In the first strategy, we enforce $\mathbf{Q} = 0$ while in the other strategy, we let \mathbf{Q} as a free parameter. For the results at $\mathbf{Q} \neq 0$, these two strategies yield the energy difference between the FFLO ground state and the possible BCS superfluid excited state, which is crucial for the stability of the FFLO phase at finite temperature.

Because the Zeeman field is applied along the x -axis, the population imbalance should be defined us-

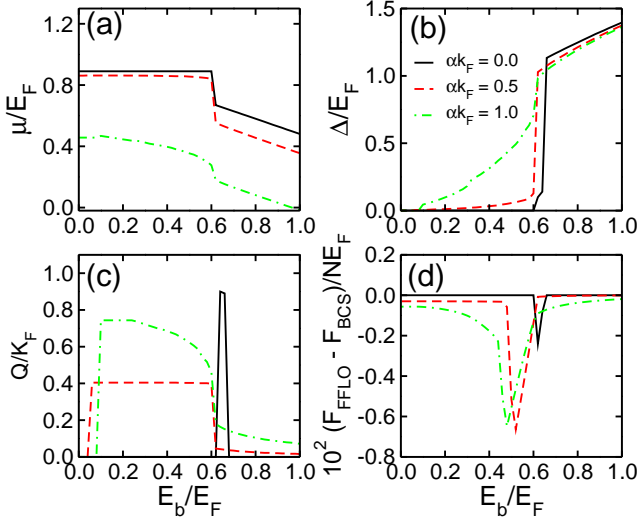


FIG. 5: (Color online). Evolution of chemical potential (a), order parameter (b), and FFLO vector \mathbf{Q} (c) as a function of the binding energy. In (d) we plot $(F_{\text{FFLO}} - F_{\text{BCS}})/nE_F$ vs. E_b . In all calculations we set $h = 0.8E_F$.

ing the eigenstates of σ_x , instead of σ_z . Since $\langle \sigma_x \rangle = \sum_{\mathbf{k}} \langle c_{\mathbf{k},\uparrow}^\dagger c_{\mathbf{k},\downarrow} + \text{h.c.} \rangle$, we therefore have

$$P = \frac{\langle \sigma_x \rangle}{n} = \frac{1}{2n} \sum_{\mathbf{k}, \lambda} \psi_{\mathbf{k}, \mathbf{Q}, \lambda}^\dagger \begin{pmatrix} \sigma_x & 0_{2 \times 2} \\ 0_{2 \times 2} & -\sigma_x \end{pmatrix} \psi_{\mathbf{k}, \mathbf{Q}, \lambda}$$

$$= \frac{1}{n} \sum_{\mathbf{k}} \psi_{\mathbf{k}, \mathbf{Q}, \lambda}^\dagger \begin{pmatrix} \sigma_x & 0_{2 \times 2} \\ 0_{2 \times 2} & 0_{2 \times 2} \end{pmatrix} \psi_{\mathbf{k}, \mathbf{Q}, \lambda}. \quad (15)$$

Here $\psi_{\mathbf{k}, \mathbf{Q}, \lambda}$ is the eigenstate of the effective Hamiltonian H_{eff} , i.e., $H_{\text{eff}} \psi_{\mathbf{k}, \mathbf{Q}, \lambda} = E_\lambda \psi_{\mathbf{k}, \mathbf{Q}, \lambda}$.

In our calculation, we choose the energy unit as the Fermi energy E_F of the system without interaction, Zeeman field and SO coupling. The corresponding length scale K_F^{-1} is defined through the Fermi momentum K_F . At finite temperature, the two dimensional system does not have the long-range order due to the phase fluctuation and the relevant physics is the Kosterlitz-Thouless transition⁵⁵. In this paper, we restrict to the physics at zero temperature, where the mean-field theory is still valid. We have numerically verify that the FFLO phase has a smaller free energy when $\mathbf{Q} // y$, as compared to that along the x direction, therefore we consider only $\mathbf{Q} = (0, Q)$. Similar conclusion can be found in three dimensional SO coupled degenerate Fermi gas, see Ref. 46, and in two dimensional superconductors where $\mathbf{Q} \perp \mathbf{B}$ for FFLO phases. We notice that the direction of the FFLO vector \mathbf{Q} is also consistent with the results in solid state systems with weak SO coupling, see Ref. 48.

III. PHASE DIAGRAM

We first present the phase diagram with different SO coupling strength and Zeeman field in Fig. 4. Without

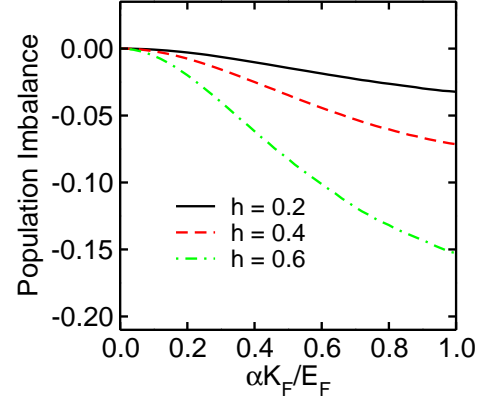


FIG. 6: (Color online). Population imbalance $P = \langle \sigma_x \rangle / n$ as a function of SO coupling strength. $E_b = 0.4E_F$.

SO coupling, see Fig. 4a, we see that the FFLO phase only exists in an extremely narrow parameter regime. When $E_b \geq 0.7E_F$, the FFLO phase disappears, thus such a phase only can be observed in the weak binding energy regime, for instance, $E_b \in (0.15, 0.7)E_F$. Similarly, the FFLO phase can also be observed in the three dimensional system, see Ref. 46. However, the FFLO phase in three dimensional Fermi gases can only be observed near the unitary regime within a small parameter region, and the small FFLO regime can be easily missed out in realistic experiments, which is also one of the main reasons why the FFLO phases cannot be observed in recent experiments in three dimensional Fermi gases²⁷⁻²⁹. With an increasing SO coupling strength, see Fig. 4b for $\alpha K_F = 0.5E_F$ and Fig. 4c for $\alpha K_F = 1.0E_F$, we find that the FFLO phase regime is greatly enlarged. In the strong SO regime in Fig. 4c, we even observe that the phase diagram is almost fully filled by the FFLO phase, while the BCS superfluid phase is greatly suppressed and only survives in a very small regime. To see the impact of SO coupling more clearly, we plot in Fig. 4d the phase diagram in the $h - \alpha K_F$ plane with $E_b = 0.4E_F$. We define the boundary between BCS superfluid and FFLO phase as h_1 and the boundary between FFLO phase and normal gas as h_2 for convenience, see Fig. 4d. We observe h_1 decreases while h_2 increases with the increasing SO coupling strength, therefore the FFLO phase is greatly enlarged in the strong SO coupling regime. It should be noticed that in three dimensional Fermi gases h_2 slightly decreases with the increasing SO coupling strength⁴⁶. In the strong SO coupling region, h_1 becomes very small, but never becomes zero because the the Zeeman field is essential for the FFLO phase, which breaks the time-reversal symmetry.

We plot the evolution of chemical potential, order parameter and Q as a function of binding energy in Fig. 5, where the Zeeman field is fixed to $h = 0.8E_F$. As we decreases the binding energy, we observe a sudden drop of the order parameter in Fig. 5b at zero SO coupling strength due to the Pauli paramagnetic depairing

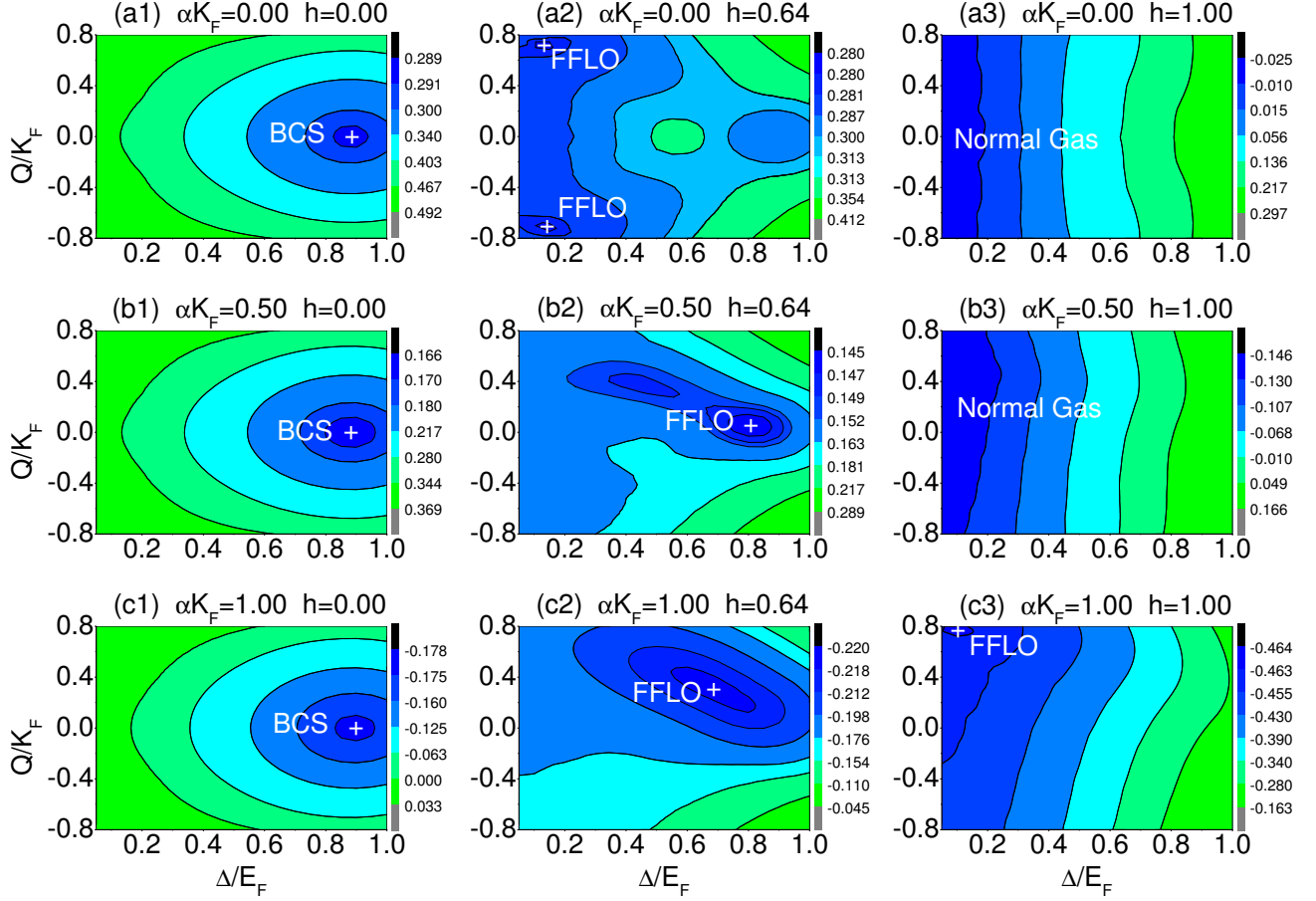


FIG. 7: (Color online). Influence of SO coupling and in-plane Zeeman field on the free energy per particle, $F/(nE_F)$, in the $Q - \Delta$ plane. The cross symbol in each panel corresponds to the self-consistent solution of Eq. 14. In (a3) and (b3) only normal gas can be observed, thus $\Delta = 0$, and Q can be any value because it doesn't enter the free energy.

effect, following which there is a small regime that supports FFLO phase, see also the solid line in Fig. 5c, $Q \neq 0$. With the increasing SO coupling strength, we see that the change of Δ becomes a smooth function of E_b , and in a much larger parameter regime we can observe the FFLO phase with non-zero Q . The decrease of the order parameter in the FFLO phase regime tends to reduce the free energy, therefore in Fig. 2 the arrows always move toward the direction with smaller order parameters with the generation of the FFLO phase.

We further consider the free energy

$$F = \Omega + n\mu, \quad (16)$$

where Ω is the thermodynamical potential defined in Eq. 11, regularized by Eq. 13. We denote F_{FFLO} as the free energy obtained by letting \mathbf{Q} as a free parameter, while F_{BCS} as the free energy by enforcing $\mathbf{Q} = 0$. In the FFLO phase regime, F_{BCS} represents the free energy of BCS excited states, therefore the energy difference per particle between F_{FFLO} and F_{BCS} , i.e., $\delta F = (F_{\text{FFLO}} - F_{\text{BCS}})/nE_F$ characterizes the stability of the FFLO phase (i.e., the larger $|\delta F|$, the more

stable FFLO phase). The numerical results are presented in Fig. 5d, where we clearly see the enhancement of $|\delta F|$ due to the SO coupling. Note that in two dimensional Fermi gases the enhanced factor is about 3, which is much smaller than that in three dimensional Fermi gases (~ 100).

In Fig. 5b, we see that in the BCS superfluid regime ($E_b > 0.7E_F$), the order parameter decreases with the increasing SO coupling, which is in sharp contrast to that for SO coupled BEC-BCS crossover with Z direction Zeeman field. Generally, with the Z direction Zeeman field, the SO coupling plays the role of increasing the density of states near the Fermi surface, which increases the order parameters as well as the critical temperature. With an in-plane Zeeman field, the SO coupling plays a totally different role. To see this more clearly, we plot the population imbalance $P = \langle \sigma_x \rangle / n$ as a function of SO coupling in Fig. 6. We see that the SO coupling generally increases the population imbalance, thus renders the decrease of the order parameter as observed in Fig. 5b, which also hinders the appearance of topological superfluid. In the FFLO phase regime, the order parameter

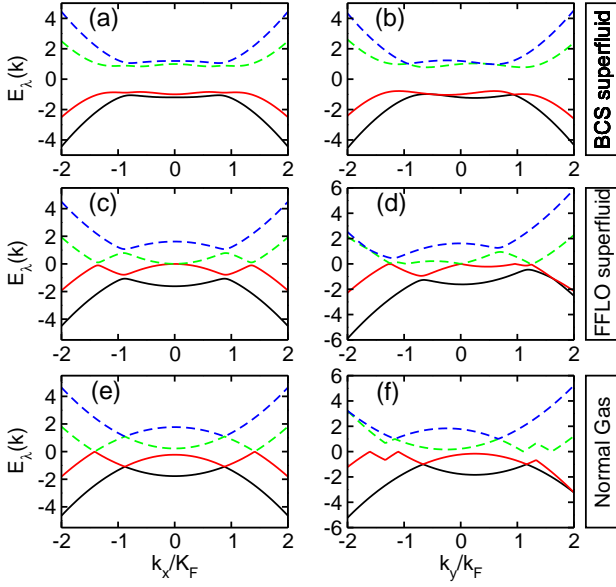


FIG. 8: (color online). Eigenvalues E_λ ($\lambda = 1, 2, 3, 4$) of the SO coupled degenerate Fermi gas. (a), (b) correspond to the typical eigenvalues E_λ for the BCS superfluid with parameters $h = 0.2$, $E_b = 0.4$, $\alpha k_F = 1.0$. (c), (d) correspond to the typical eigenvalues E_λ for the FFLO superfluid with parameters $h = 0.4$, $E_b = 0.4$, $\alpha k_F = 1.0$. (e), (f) correspond to the typical eigenvalues E_λ for the normal gas with parameters $h = 1.0$, $E_b = 0.4$, $\alpha k_F = 1.0$. The first column shows the results along the x direction, while the second column shows the results along the y direction.

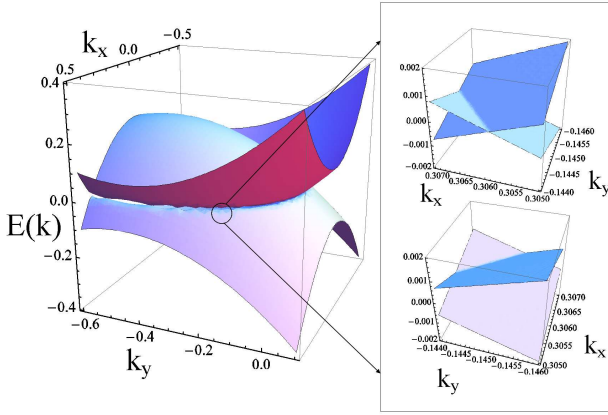


FIG. 9: Gapless excitations for the FFLO phase. Near $E_{k,\lambda} = 0$, the dispersion show clear linear dispersion. In two dimensional system the linear dispersion is essential to make the FFLO phase robust against low-energy fluctuations.

increases with the increasing SO coupling strength due to the formation of the FFLO phase.

The basic physical picture in Fig. 1b represents a totally different and more efficient route to find the FFLO state. However, the physical picture along is insufficient to explain the emergence of the FFLO phase. To understand the results more clearly, we plot the free energy per

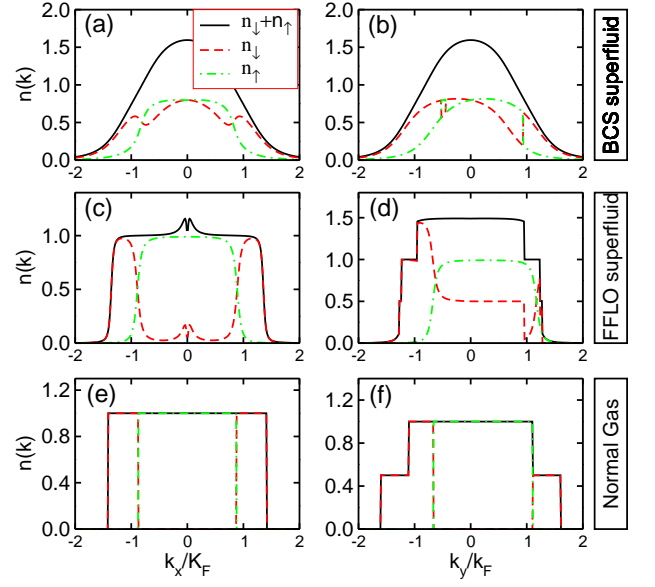


FIG. 10: (color online). Momentum distributions $n_\sigma(k) = \langle c_\sigma^\dagger(k) c_\sigma(k) \rangle$ and $n = n_\downarrow + n_\uparrow$ for different quantum phases. Other parameters are exactly the same as that in Fig. 8.

particle in the $Q - \Delta$ plane, where the global minimum of the free energy marked by the cross symbol in each panel corresponds to the self-consistent solution of Eq. 14. The left to right shows the influence of the SO coupling on the formation of the FFLO phase, while the top to down shows the influence of the Zeeman field. Note that without SO coupling, the free energy is a symmetric function of Q , therefore in Fig. 7a2 there are two degenerate FFLO ground states at $\pm Q$ because we have assumed \mathbf{Q} is along the y direction in our numerical simulation. This is not true in the real system because the free energy only depends on the magnitude of $|Q|$, but is independent of the direction of Q due to the rotation symmetry, see Eq. 1. The free energy is still a symmetric function with respect to Q when $h = 0$. However it becomes an asymmetric function when both Zeeman field and SO coupling strength become non-zero, thus only one global minimum can be found in the $Q - \Delta$ plane in Figs. 7b2, c2, c3, and the ground state is unique. The plot of the free energy in the $Q - \Delta$ plane reflects the effect of the symmetry of the effective Hamiltonian, see also Appendix A. With the increasing Zeeman field, the order parameter decreases due to the formation of the FFLO phase, which is in consistent with the basic physical picture in Fig. 2. Due to the increase of h_2 , the boundary between FFLO phase and normal gas, we observe the FFLO phase in the strong Zeeman field and strong SO coupling region in Fig. 7c3.

IV. MEASUREMENT OF THE FFLO PHASE

The three different phases have different properties which can be used for the identification of these phases. In Fig. 8, we plot the typical band structures E_λ , $\lambda = 1, 2, 3, 4$, for the BCS superfluid, the FFLO phase and the normal gas. Due to the rotational symmetry breaking, we have to plot the dispersions along the k_x and k_y axes, respectively. For a typical BCS superfluid ($\mathbf{Q} = 0$) in Fig. 8a and Fig. 8b, we see that the system is always gapped and the band structure is always symmetric about $\mathbf{k} = 0$ for the dispersion along k_x . While along the k_y axis, such symmetry is absent. For the BCS superfluid we can prove that when $\hbar^2 < \Delta^2$ and $\Delta \neq 0$, the BCS superfluid is always gapped, see Appendix A. However for the FFLO phase, the superfluid becomes gapless along both k_x and k_y axes. Along the k_x axis the band structure is symmetric about $\mathbf{k} = 0$, but along the k_y direction such symmetry is broken. For the FFLO phase we observe $\sum_\lambda E_\lambda \neq 0$ because $\mathbf{Q} \neq 0$, which is consistent with our symmetry analysis in Appendix A. In fact, gapless excitations are a typical feature of the FFLO phase, as have been pointed out in literature^{24,61}. In the vicinity of the gapless excitation, see Fig. 9, the dispersion becomes linear which is essential to ensure that the FFLO phase is robust against the low-energy fluctuations. Here we should emphasize that not all FFLO phases are gapless. The FFLO state may become gapless only when Q is relatively large, while for a small Q (near the boundary between FFLO and BCS superfluid) the FFLO phase is still gapped, similar to that in the BCS superfluid. For the normal gas the band structure also shows strong asymmetry along the k_y axis, as seen in Fig. 8e and Fig. 8f.

The corresponding momentum distributions $n_\sigma = \langle c_{k\sigma}^\dagger c_{k\sigma} \rangle$ and $n = n_\uparrow + n_\downarrow$ provide an important tool to detect the properties of the FFLO state because they can be directly measured via free expansion of the cloud. We plot the momentum distributions in Fig. 10 for the three different phases presented in Fig. 8 at zero temperature. The dispersion properties of the band structures can be directly reflected on the corresponding momentum distributions. We see that for three different quantum phases, the momentum distributions are always symmetric about $\mathbf{k} = 0$ along the k_x direction, while show strong asymmetric along the k_y direction. However, the sum of the momentum distributions n for spin up and spin down components still shows perfect symmetry about $\mathbf{k} = 0$ along both k_x and k_y directions. Therefore detecting the asymmetry of the superfluid is not sufficient for the identification of the FFLO phase. To identify the superfluid nature of the FFLO phase, we have to rotate the sample to create vortices, which is a direct evidence of superfluidity. Near the boundary between different phases, the fluctuation effect may become significant thus the phase boundary region is not suitable for the observation of vortices. With the large FFLO phase region in our model we can safely choose some parameters in the middle of the FFLO phase where the fluctuation effect should be min-

imized. The large FFLO superfluid phase ensures that it will not be missed out in future realistic experiments.

The properties of the FFLO phase may be measured using a number of methods developed in ultracold atom systems, for instance, shot-noise correlation⁶² and density-density correlation measurement^{63,64}, which show a peak at the Cooper pair momentum \mathbf{Q} . After released from a trapping potential, the free expansion of the Fermi cloud has a peak at $\mathbf{r} = \hbar\mathbf{Q}t/m$, therefore the direct measurement of the FFLO momentum \mathbf{Q} is possible⁶⁵. In our model when \mathbf{Q} is unique, repeated measurement to determine the FFLO momentum becomes possible. In the FFLO phase without SO coupling, the ground states is independent of the direction of \mathbf{Q} , then such measurement may become difficult. The FFLO phase can also be measured using the Fourier sampling of time-of-flight images proposed by Duan⁶⁶. The gapless excitations in the FFLO phase may be observed using the Bragg spectroscopy⁶⁵.

V. CONCLUSION

To summarize, in this paper, we study the possible FFLO phase in SO coupled degenerate Fermi gases with in-plane Zeeman fields. We show that the FFLO phase can be greatly enlarged due to the deformation of the Fermi surface. The emergence of the FFLO phase is understood from different angles. The properties of the BCS superfluid, FFLO phase and normal gas have also been discussed and their measurement through the time-of-flight imaging is presented. The deformation of the Fermi surface provides a more efficient method to generate the FFLO phase. On the experimental side, the SO coupling has been realized in Bose³⁸⁻⁴¹ and Fermi^{42,43} gases, while the later is more relevant to the topics in this work. Moreover, the in-plane Zeeman field can be naturally created^{38-40,42,43} and controlled at will, thus we expect the idea in this work may provide a path for elucidating the long-standing problem about FFLO phases in experiments in the near future.

Acknowledgement: Z.Z., X.Z., and G.G. are supported by the National 973 Fundamental Research Program (Grant No. 2011cba00200), the National Natural Science Foundation of China (Grant No. 11074244 and No. 11274295). M.G. and C.Z. are supported by ARO (W911NF-12-1-0334), DARPA-YFA (N66001-10-1-4025), and NSF-PHY (1104546).

Appendix A: Symmetry of the effective Hamiltonian

The symmetry of the effective Hamiltonian is one of the major concerns in this work. In the following, we discuss the symmetry difference between the out-of-plane and in-plane Zeeman field models. We consider the following

generalized effective model,

$$H_{\text{eff}} = \begin{pmatrix} \mathcal{K}(\mathbf{k}) & \Delta I_{2 \times 2} \\ \Delta^\dagger I_{2 \times 2} & -\sigma_y \mathcal{K}^*(-\mathbf{k}) \sigma_y \end{pmatrix} \quad (\text{A1})$$

with

$$\mathcal{K}(\mathbf{k}) = \begin{pmatrix} \xi_{\mathbf{k}+\mathbf{Q}/2,\uparrow} & h - \alpha R(\mathbf{k}) \\ h - \alpha R(\mathbf{k})^* & \xi_{\mathbf{k}+\mathbf{Q}/2,\downarrow} \end{pmatrix}, \quad (\text{A2})$$

where $\xi_{\mathbf{k}\sigma} = \frac{\mathbf{k}^2}{2m} - \mu + \sigma\Gamma$. We have applied Zeeman fields along Z direction and X direction simultaneously.

Here we only analyze the symmetry of the BCS superfluid in the generalized model in Eq. A1, which is more relevant to topological excitations such as zero-energy Majorana Fermions in vortex cores of the superfluid. We hence set $\mathbf{Q} = 0$. For the case with only out-of-plane Zeeman field, we set $h = 0$. The SO coupling term can be written as $V_{\text{so}} = \alpha(k_x \sigma_y - k_y \sigma_x)$, therefore we define

$$\begin{pmatrix} -k'_y \\ k'_x \end{pmatrix} = U \begin{pmatrix} -k_y \\ k_x \end{pmatrix}, \quad \begin{pmatrix} \sigma'_x \\ \sigma'_y \end{pmatrix} = U \begin{pmatrix} \sigma_x \\ \sigma_y \end{pmatrix}, \quad (\text{A3})$$

where U is the $\text{SU}(2)$ rotation matrix that takes the following form,

$$U = \begin{pmatrix} \cos(\theta) & \sin(\theta) \\ -\sin(\theta) & \cos(\theta) \end{pmatrix}. \quad (\text{A4})$$

We can easily verify that $UU^\dagger = 1$, therefore $\xi_{\mathbf{k}'\sigma} = \xi_{\mathbf{k}\sigma}$. On the other hand by defining $\sigma'_z = \sigma_z$, we find the new Pauli matrices $\sigma'_{x,y,z}$ satisfy the standard commutation relations

$$[\sigma'_a, \sigma'_b] = 2i \sum_c \varepsilon_{abc} \sigma'_c, \quad \{\sigma'_a, \sigma'_b\} = 2\delta_{ab} \quad (\text{A5})$$

with ε_{abc} the Levi-Civita symbol and δ_{ab} the Kronecker delta. The rotational symmetry plus the particle-hole symmetry ensure that the eigenvalues at each \mathbf{k} should appear in pairs, thus in the topological superfluid regime, the lowest non-negative eigenvalue and the highest non-positive eigenvalue can become zero simultaneously and the Majorana Fermions are created in the vortex core of the topological superfluid.

The above analysis cannot be applied to the case when $h \neq 0$. Actually the in-plane magnetic field breaks the rotational symmetry of the effective Hamiltonian, because under the rotational symmetry in Eq. A4, we have the following transformation,

$$h\sigma_x \rightarrow h(\cos(\theta)\sigma_x + \sin(\theta)\sigma_y). \quad (\text{A6})$$

The breakdown of the rotational symmetry makes the superfluid asymmetric, rendering the unique FFLO vector \mathbf{Q} , which is one of the major advantages of our proposal. The unique \mathbf{Q} makes the detection of the FFLO vector more easily in realistic experiments, as discussed in the main text in sec. IV.

The topological properties of the BCS superfluid can be calculated from the Pfaffian of the following matrix

$$W(\mathbf{k}) = H_{\text{eff}}(\mathbf{k})\Lambda = H_{\text{eff}}(\mathbf{k}) \begin{pmatrix} 0 & -i\sigma_y \\ i\sigma_y & 0 \end{pmatrix}. \quad (\text{A7})$$

Notice that the particle-hole symmetry $\Lambda H_{\text{eff}}^*(\mathbf{k})\Lambda = -H_{\text{eff}}(-\mathbf{k})$, where $\Lambda = \Lambda^T = \Lambda^\dagger$, thus $H_{\text{eff}}^*(\mathbf{k})\Lambda = -\Lambda H_{\text{eff}}(-\mathbf{k})$, and $\Lambda^\dagger H_{\text{eff}}^T(\mathbf{k}) = -H_{\text{eff}}^\dagger(-\mathbf{k})\Lambda^\dagger = -H_{\text{eff}}(-\mathbf{k})\Lambda^\dagger$. We have

$$W^T(\mathbf{k}) = \Lambda^T H_{\text{eff}}^T(\mathbf{k}) = \Lambda^\dagger H_{\text{eff}}(-\mathbf{k})\Lambda^\dagger = -W(-\mathbf{k}). \quad (\text{A8})$$

When $\mathbf{k} = 0$, we see $W(\mathbf{k})$ is an antisymmetric matrix. As has been shown in Ref. 52, the topological phase transition is determined by the Pfaffian of $W(\mathbf{k})$ at $\mathbf{k} = 0$.

The Pfaffian of the antisymmetric matrix $W(\mathbf{k})$ is directly related to the topological invariance of the system. Define

$$Q[H_{\text{eff}}(\mathbf{k})] = \text{sign}(\text{Pf}(W(\mathbf{k}))). \quad (\text{A9})$$

We see $Q = \pm 1$. Notice that $\text{Pf}(A)^2 = \text{Det}(A)$ where A is any anti-symmetric matrix, and

$$\text{Pf}(H_{\text{eff}}(\mathbf{k})\Lambda)^2 = \text{Det}(H_{\text{eff}}(\mathbf{k})\Lambda) = \text{Det}(H_{\text{eff}}(\mathbf{k})). \quad (\text{A10})$$

Therefore Q changes sign only when $\text{Det}(H_{\text{eff}}(\mathbf{k})) = 0$. The deformation to the effective Hamiltonian generally does not change the value of Q , thus Q is topologically invariant. When $\mathbf{k} = 0$ and $\mathbf{Q} = 0$ (for BCS superfluid), we have

$$Q[H_{\text{eff}}(\mathbf{k} = 0)] = \text{sign}(h^2 + \Gamma^2 - (\mu^2 + \Delta^2)). \quad (\text{A11})$$

Thus for an in-plane Zeeman field, the system still has a topological phase transition, where the phase transition takes place at $h^2 + \Gamma^2 = \Delta^2 + \mu^2$, at which point the band gap at \mathbf{k} closes. We recover the well-known results when Zeeman field is set along the Z direction. Notice that in our model the order parameter and chemical potential should be determined self-consistently, where the Zeeman field generally destroys the superconductivity when $h^2 + \Gamma^2 > \Delta^2$, therefore the existence of the topological superfluid is not straightforward.

We define the product of the eigenvalues,

$$F = \prod_\lambda E_\lambda = \text{Det}(H_{\text{eff}}). \quad (\text{A12})$$

For the system with the rotational symmetry ($h = 0$), we have

$$F = (h^2 + \alpha^2 k^2 - \Delta^2 - \xi_{\mathbf{k}}^2)^2 + 4\alpha^2 k^2 \Delta^2 \geq 0. \quad (\text{A13})$$

Obviously, $F = 0$ happens at $\mathbf{k} = 0$ and $\Gamma^2 = \Delta^2 + \mu^2$. When $h \neq 0$, we find

$$F = (h^2 - (\Delta^2 + A - 2\sqrt{B}))(h^2 - (\Delta^2 + A + 2\sqrt{B})). \quad (\text{A14})$$

Therefore $F = 0$ gives

$$h^2 = \Delta^2 + A \pm 2\sqrt{B}, \quad (\text{A15})$$

where $A = \xi_{\mathbf{k}}^2 + \alpha^2(k_y^2 - k_x^2) - \Gamma^2$, and $B = \alpha^2 k_y^2 (\xi_{\mathbf{k}}^2 - \Gamma^2) - \alpha^2 k_x^2 (\Delta^2 + \alpha^2 k_y^2)$. When $B \leq 0$, F is always large than zero and the system is always gapped. We can easily verify that there is no real solution for $A < 0$ and $B > 0$, therefore $A > 0$. Moreover, we find

$$A^2 - 4B = (\Gamma^2 - \xi^2 - \alpha^2(k_x^2 + k_y^2))^2 + 4\alpha^2 k_x^2 \Delta^2 \geq 0. \quad (\text{A16})$$

Hence $A - 2\sqrt{B} \geq 0$ and $h^2 \geq \Delta^2$ when the system has potential zero eigenvalues. Notice that for topological superfluid, $h^2 > \Delta^2 + \mu^2$ is required. We find numerically that before reaching the regime $h^2 \geq \Delta^2$, the superfluid is always destroyed. Therefore for the BCS superfluid the system is always gapped and the topological phase transition can never happen. Notice that in our system the order parameter and chemical potential should be obtained self-consistently by solving the number and gap equations, therefore the existence of the topological superfluid is not straightforward.

The sum of the eigenvalues has the following identity

$$\text{Tr}(H_{\text{eff}}) = \sum_{\lambda} E_{\mathbf{k},\lambda} = \frac{2\mathbf{k} \cdot \mathbf{Q}}{m}. \quad (\text{A17})$$

Therefore for the BCS superfluid the sum of the eigenvalues should be exactly zero, while for the FFLO superfluid the sum will never be equal zero, which means that for FFLO superfluid, the eigenvalues will never appear in pairs $(E, -E)$. The above two results mark the important feature of the in-plane Zeeman field which differs dramatically from the Z direction Zeeman field. This is a direct consequence of rotational symmetry breaking due to the in-plane Zeeman field.

Appendix B: Quantum Field Theory

To facilitate the future investigation of the FFLO phase in ultracold atomic systems, we present the standard field treatment of the FFLO phase in SO coupled degenerate Fermi gases. The same results in this appendix have been obtained using the mean-field theory in the main text and these two methods give consistent description of the FFLO physics. The quantum field theory has the potential of incorporating the fluctuation effect thus can be used in the future for studying the physics at finite temperature.

The partition function at finite temperature reads as

$$Z = \int \mathcal{D}[\psi, \psi^\dagger] e^{-S[\psi, \psi^\dagger]}, \quad (\text{B1})$$

where

$$S[\psi, \psi^\dagger] = \int d\tau d\mathbf{r} \sum_{\sigma=\uparrow,\downarrow} \psi_\sigma(\mathbf{x})^\dagger \partial_\tau \psi_\sigma(\mathbf{x}) + H, \quad (\text{B2})$$

where $H = H_0 + V_{\text{int}}$, with

$$H_0 = \sum_{\sigma, \sigma'=\uparrow,\downarrow} \psi_\sigma^\dagger \underbrace{\left(\frac{p^2}{2m} - \mu + V_{\text{so}} + h\sigma_x \right)}_{H_{\sigma\sigma'}} \psi_{\sigma'}, \quad (\text{B3})$$

$V_{\text{so}} = \alpha(p_x \sigma_y - p_y \sigma_x)$, and

$$V_{\text{int}} = g \psi_\uparrow^\dagger \psi_\downarrow^\dagger \psi_\downarrow \psi_\uparrow. \quad (\text{B4})$$

Here we assume a contact interaction, i.e., the two-particle interaction $V(\mathbf{x}, \mathbf{y}) = g\delta(\mathbf{x} - \mathbf{y})$ with g as the renormalized interaction strength. The FFLO order parameter is

$$g\langle \psi_\downarrow(\mathbf{x}) \psi_\uparrow(\mathbf{x}) \rangle = \Delta e^{i\mathbf{Q} \cdot \mathbf{x}}, \quad (\text{B5})$$

where \mathbf{Q} is the total momentum of the Cooper pairs, and Δ is a spatially independent constant. We make the following transformation,

$$\psi_\sigma \rightarrow \psi_\sigma e^{i\mathbf{Q} \cdot \mathbf{x}/2} \quad (\text{B6})$$

to remove the extra phase factor in the real space order parameter. Here we should emphasize that, in principle, we can assume $\psi_\sigma \rightarrow \psi_\sigma e^{i\mathbf{Q}_\sigma \cdot \mathbf{x}}$, where $\mathbf{Q}_\uparrow + \mathbf{Q}_\downarrow = \mathbf{Q}$ to make the pairing position independent. All these different choices of the \mathbf{Q}_i are equivalent class albeit the effective Hamiltonian may be totally different. This property can be seen very clearly using the quantum field theory, but cannot be seen using the mean field developed in the main text. This flexibility may offer some advantage in dealing with some particular problems, however for the model considered in this work, we find $\mathbf{Q}_\uparrow = \mathbf{Q}_\downarrow$ gives the simplest expression for the effective Hamiltonian, which is exactly the same as what we have obtained in the main text. For the single particle Hamiltonian, we find,

$$\psi_\sigma^\dagger H_{\sigma\sigma'}(\mathbf{p}) \psi_{\sigma'} \rightarrow \psi_\sigma^\dagger e^{-i\mathbf{Q} \cdot \mathbf{x}/2} H_{\sigma\sigma'}(\mathbf{p}) e^{i\mathbf{Q} \cdot \mathbf{x}/2} \psi_{\sigma'}. \quad (\text{B7})$$

Thus we have the following transformation,

$$\begin{aligned} H_{\sigma\sigma'}(\mathbf{p}) &\rightarrow e^{-i\mathbf{Q} \cdot \mathbf{x}/2} H_{\sigma\sigma'}(\mathbf{p}) e^{i\mathbf{Q} \cdot \mathbf{x}/2} \\ &= H_{\sigma\sigma'}(\mathbf{p} + \mathbf{Q}/2). \end{aligned} \quad (\text{B8})$$

The action without many-body interaction therefore reads as

$$S_0[\psi, \psi^\dagger] = \int d\tau d\mathbf{r} \sum_{\sigma=\uparrow,\downarrow} \psi_\sigma^\dagger \partial_\tau \psi_\sigma + \psi_\sigma^\dagger H_{\sigma\sigma'}(\mathbf{p} + \frac{\mathbf{Q}}{2}) \psi_{\sigma'}, \quad (\text{B9})$$

which means that we just need to replace \mathbf{p} with $\mathbf{p} + \mathbf{Q}/2$, and, $-\mathbf{p}$ with $-\mathbf{p} + \mathbf{Q}/2$ so as to construct the effective Hamiltonian. Using the standard Hubbard-Stratanovich transformation,

$$\begin{aligned} \exp(-g \int d\mathbf{x} d\tau \psi_\downarrow^\dagger \psi_\uparrow^\dagger \psi_\uparrow \psi_\downarrow) &= \int \mathcal{D}[\Delta] \times \\ \exp(\int d\tau d\mathbf{x} \frac{\Delta \Delta^*}{g} + \Delta \psi_\downarrow^\dagger \psi_\uparrow^\dagger + \Delta^* \psi_\uparrow \psi_\downarrow), \end{aligned} \quad (\text{B10})$$

the Fermi field now becomes quadratic thus can be integrated out, leaving only the bosonic field Δ and its conjugate. The partition function $Z = \int \mathcal{D}\Delta e^{-S_{\text{eff}}}$, where the effective action reads as,

$$S_{\text{eff}} = \int d\tau d\mathbf{r} \frac{|\Delta|^2}{g} - \frac{1}{2\beta} \ln \text{Det} \beta G^{-1} + \text{Tr}(H), \quad (\text{B11})$$

where $\beta = 1/T$, $\text{Tr}(H) = \sum_{\sigma} H_{\sigma\sigma}$, and $G^{-1} = \partial_{\tau} + H_{\text{eff}}$, with the effective Hamiltonian

$$H_{\text{eff}} = \begin{pmatrix} \mathcal{K}(\mathbf{p}) & \Delta I_{2 \times 2} \\ \Delta^{\dagger} I_{2 \times 2} & -\sigma_y \mathcal{K}^*(-\mathbf{p}) \sigma_y \end{pmatrix}. \quad (\text{B12})$$

Here

$$\mathcal{K}(\mathbf{p}) = \begin{pmatrix} H_{\uparrow\uparrow}(\mathbf{p} + \mathbf{Q}/2) & H_{\uparrow\downarrow}(\mathbf{p} + \mathbf{Q}/2) \\ H_{\downarrow\uparrow}(\mathbf{p} + \mathbf{Q}/2) & H_{\downarrow\downarrow}(\mathbf{p} + \mathbf{Q}/2) \end{pmatrix}. \quad (\text{B13})$$

The basis is arranged as $(\psi_{\uparrow}, \psi_{\downarrow}, \psi_{\downarrow}^{\dagger}, -\psi_{\uparrow}^{\dagger})$. The above Hamiltonian is also identical to the effective Hamiltonian in Eq. 8 in the main text. For the particle-hole symmetry of the above Hamiltonian, see the discussion in the main text.

For the saddle point approximation, we assume $\Delta = \Delta_0 + \eta$, where Δ_0 is spatially independent, while $\eta = \eta(\mathbf{x})$ corresponds to the fluctuation field. The contribution of the fluctuation field is not considered here, thus to the leading order, we have the effective action

$$S_{\text{eff}} = -\beta \frac{|\Delta_0|^2}{g} - \frac{1}{2} \sum_{\mathbf{k}, \lambda, i\omega} \ln(\beta(i\omega - E_{\lambda})) + \beta \sum_{\mathbf{k}} \xi_{\mathbf{k}}, \quad (\text{B14})$$

where $i\omega = (2n+1)\pi T$ is the Matsubara frequency. E_{λ} is the eigenvalue of the effective Hamiltonian H_{eff} . Summing over the Matsubara frequency using the standard method and the relationship between effective action and thermodynamical potential $\Omega = S_{\text{eff}}/\beta = S_{\text{eff}}T$, we have

$$\Omega = -\frac{|\Delta_0|^2}{g} - \frac{1}{2\beta} \sum_{\mathbf{k}, \lambda} \ln(1 + e^{-E_{\beta\lambda}}) + \sum_{\mathbf{k}} \xi_{\mathbf{k}}. \quad (\text{B15})$$

At zero temperature, we have

$$\begin{aligned} \lim_{T \rightarrow 0^+} T \ln(1 + e^{-E/T}) &= \begin{cases} 0 & E \geq 0, \\ -E & E < 0. \end{cases} \\ &= -E\Theta(-E), \end{aligned} \quad (\text{B16})$$

where $\Theta(x)$ is the Heaviside step function. Thus we have

$$\Omega = -\frac{|\Delta_0|^2}{g} + \frac{1}{2} \sum_{\mathbf{k}, \lambda} E_{\lambda} \Theta(-E_{\lambda}) + \sum_{\mathbf{k}} \xi_{\mathbf{k}}. \quad (\text{B17})$$

We hereby recover the results from the mean field theory in Eq. 11.

* Email: skylark.gong@gmail.com

† Email: xbz@ustc.edu.cn

‡ Email: chuanwei.zhang@utdallas.edu

¹ J. Bardeen, L. N. Cooper, and J. R. Schrieffer, Phys. Rev. **106**, 162 (1957).

² P. Fulde, and R. A. Ferrell, Phys. Rev. **135**, A550 (1964).

³ A. I. Larkin, and Yu. N. Ovchinnikov, Zh. Eksp. Teor. Fiz. **47**, 1136 (1964).

⁴ A. I. Larkin, and Yu. N. Ovchinnikov, Sov. Phys. JETP **20**, 762 (1965).

⁵ A. Buzdin, Y. Matsuda, and T. Shibauchi, Europhys. Lett., **80**, 67004 (2007).

⁶ M. D. Croitoru, M. Houzet and A. I. Buzdin, Phys. Rev. Lett. **108**, 207005 (2012).

⁷ Y. Matsuda, and H. Shimahara, J. Phys. Soc. Jpn. **76**, 051005 (2007).

⁸ K. Gloos, R. Modler, H. Schimanski, C. D. Bredl, C. Geibel, F. Steglich, A. I. Buzdin, N. Sato, and T. Komatsubara, Phys. Rev. Lett. **70**, 501 (1993).

⁹ A. Bianchi, R. Movshovich, C. Capan, P. G. Pagliuso, and J. L. Sarrao, Phys. Rev. Lett. **91**, 187004 (2003).

¹⁰ J. Singleton, J. A. Symington, M-S Nam, A. Ardavan, M. Kurmoo, and P. Day, J. Phys.: Condens. Matter **12**, L641 (2000).

¹¹ R. Lortz, Y. Wang, A. Demuer, P. H. M. Böttger, B. Bergk, G. Zwicknagl, Y. Nakazawa, and J. Wosnitza, Phys. Rev. Lett. **99**, 187002 (2007).

¹² R. Casalbuoni and G. Narduli, Rev. Mod. Phys. **76**, 263 (2004).

¹³ M. G. Alford, K. Rajagopal, T. Schaefer, A. Schmitt, Rev. Mod. Phys. **80**, 1455 (2008).

¹⁴ M. Houzet and A. Buzdin, Phys. Rev. B **63**, 184521 (2001).

¹⁵ L. G. Alsamzov, Zh. Eksp. Teor. Fiz. **55**, 1477 (1968) [Sov. Phys. JETP **28**, 773 (1969)].

¹⁶ A. V. Balatsky, I. Vekhter, J.-X. Zhu, Rev. Mod. Phys. **78**, 373 (2006).

¹⁷ M. W. Zwierlein, C. A. Stan, C. H. Schunck, S. M. F. Raupach, A. J. Kerman, and W. Ketterle, Phys. Rev. Lett. **92**, 120403 (2004).

¹⁸ C. Chin, R. Grimm, P. Julienne, and E. Tiesinga, Rev. Mod. Phys. **82**, 1225 (2010).

¹⁹ S. Giorgini, L. P. Pitaevskii, and S. Stringari, Rev. Mod. Phys. **80**, 1215 (2008).

²⁰ P. Horak, J. Y. Courtois, G. Grynberg, Phys. Rev. A **58**, 3953 (1998).

²¹ L. Guidoni, C. Triché, P. Verkerk, and G. Grynberg, Phys. Rev. Lett. **79**, 3363 (1997).

²² L. Sanchez-Palencia and M. Lewenstein, Nature Physics **6**,

- 87 (2010).
- ²³ M.W. Zwierlein, J. R. Abo-Shaeer, A. Schirotzek, C.H. Schunck, and W. Ketterle, *Nature* **435**, 1047 (2005).
 - ²⁴ D. E. Sheehy and L. Radzihovsky, *Phys. Rev. Lett.* **96**, 060401 (2006).
 - ²⁵ Y. L. Loh and N. Trivedi, *Phys. Rev. Lett.* **104**, 165302 (2010).
 - ²⁶ H. Hu and X.-J. Liu, *Phys. Rev. A* **73**, 051603(R) (2006).
 - ²⁷ M. W. Zwierlein, A. Schirotzek, C. H. Schunck, and W. Ketterle, *Science* **311**, 492 (2006).
 - ²⁸ M. W. Zwierlein, C. H. Schunck, A. Schirotzek, and W. Ketterle, *Nature* **442**, 54 (2006).
 - ²⁹ G. B. Partridge, W. Li, R. I. Kamar, Y.-A. Liao and R. G. Hulet, *Science*, **311**, 503 (2006).
 - ³⁰ W. V. Liu, F. Wilczek, *Phys. Rev. Lett.* **90**, 047002 (2003).
 - ³¹ R. Winkler, *Spin-Orbit Coupling Effects in Two-Dimensional Electron and Hole Systems*, Springer Tracts in Modern Physics Vol. 191 (Springer-Verlag, Berlin, 2003).
 - ³² J. Ruseckas, G. Juzeliunas, P. öhberg, and M. Fleischhauer, *Phys. Rev. Lett.* **95**, 010404 (2005).
 - ³³ X.-J. Liu, M. F. Borunda, X. Liu, and J. Sinova, *Phys. Rev. Lett.* **102**, 046402 (2009).
 - ³⁴ X.-J. Liu, X. Liu, L. C. Kwek, and C. H. Oh, *Phys. Rev. Lett.* **98**, 026602 (2007).
 - ³⁵ C. Zhang, *Phys. Rev. A* **82**, 021607 (2010).
 - ³⁶ D. L. Campbell, G. Juzeliunas, and I. B. Spielman, *Phys. Rev. A* **84**, 025602 (2011).
 - ³⁷ J. D. Sau, R. Sensarma, S. Powell, I. B. Spielman, and S. Das Sarma, *Phys. Rev. B* **83**, 140510(R) (2011).
 - ³⁸ Y.-J. Lin, K. Jimenez-Garcia, and I. B. Spielman, *Nature* **471**, 83 (2011).
 - ³⁹ Y.-J. Lin, R. L. Compton, A. R. Perry, W. D. Phillips, J. V. Porto, and I. B. Spielman, *Phys. Rev. Lett.* **102**, 130401 (2009).
 - ⁴⁰ J.-Y. Zhang *et al.*, *Phys. Rev. Lett.* **109**, 115301 (2012).
 - ⁴¹ C. Qu, C. Hammar, M. Gong, C. Zhang, P. Engels, in preparation.
 - ⁴² P. Wang, Z.-Q. Yu, Z. Fu, J. Miao, L. Huang, S. Chai, H. Zhai, J. Zhang, *Phys. Rev. Lett.* **109**, 095301 (2012).
 - ⁴³ L. W. Cheuk, A. T. Sommer, Z. Hadzibabic, T. Yefsah, W. S. Bakr, M. W. Zwierlein, *Phys. Rev. Lett.* **109**, 095302 (2012).
 - ⁴⁴ L. He, M. Jin and P. Zhuang, *Phys. Rev. B* **74**, 024516 (2006).
 - ⁴⁵ G. J. Conduit, P. H. Conlon, B. D. Simons, *Phys. Rev. A* **77**, 053617 (2008).
 - ⁴⁶ Z. Zheng, M. Gong, X. Zou, C. Zhang and G.-C. Guo, arXiv:1208:2029.
 - ⁴⁷ J. Dalibard, F. Gerbier, G. Juzeliunas, and P. Öhberg, *Rev. Mod. Phys.* **83**, 1523 (2011).
 - ⁴⁸ V. Barzykin and L. Gor'kov, *Phys. Rev. Lett.* **89**, 227002 (2002).
 - ⁴⁹ K. Michaeli, A. C. Pooter and P. A Lee, *Phys. Rev. Lett.* **118**, 117003 (2012).
 - ⁵⁰ K. Martiyanov, V. Makhlov, and A. Turlapov, *Phys. Rev. Lett.* **105**, 030404 (2010).
 - ⁵¹ A. P. Schyder, S. Ryu, A. Furusaki, and A. W. W. Ludwig, *Phys. Rev. B* **78**, 195125 (2008).
 - ⁵² P. Ghosh, J. D. Sau, S. Tewari, and S. Das Sarma, *Phys. Rev. B* **82**, 184525 (2010).
 - ⁵³ C. Zhang, S. Tewari, R. M. Lutchyn, and S. Das Sarma, *Phys. Rev. Lett.* **101**, 160401 (2008).
 - ⁵⁴ M. Gong, S. Tewari and C. Zhang, *Phys. Rev. Lett.* **107**, 195303 (2011).
 - ⁵⁵ M. Gong, G. Chen, S. Jia, and C. Zhang, *Phys. Rev. Lett.* **109**, 105302 (2012).
 - ⁵⁶ J. Zhou, W. Zhang and W. Yi, *Phys. Rev. A* **84**, 063603 (2011).
 - ⁵⁷ M. Iskin and A. L. Subasi, *Phys. Rev. Lett.* **107**, 050402 (2011).
 - ⁵⁸ X.-J. Liu, L. Jiang, H. Pu, and H. Hu, *Phys. Rev. A* **85**, 021603(R) (2012).
 - ⁵⁹ M. Iskin, *Phys. Rev. A* **85**, 013622 (2012).
 - ⁶⁰ G. Chen, M. Gong, and C. Zhang, *Phys. Rev. A* **85**, 013601 (2012).
 - ⁶¹ C. -H. Pao, S.-T. Wu and S. -K. Yip, *Phys. Rev. B* **73**, 132506 (2006).
 - ⁶² E. Altman, E. Demler, and M. D. Lukin, *Phys. Rev. A* **70**, 013603 (2004).
 - ⁶³ T. K. Koponen, T. Paananen, J-P Martikainen, and P. Törmä, *Phys. Rev. Lett.* **99**, 120403 (2007).
 - ⁶⁴ T. K. Koponen, T. Paananen, J-P Martikainen, M. r. Bakhtiari, and P. Törmä, *New. J. Phys.* **10**, 045014 (2008).
 - ⁶⁵ J. Steinhauer, N. Katz, R. Ozeri, N. Davidson, C. Tozzo, F. Dalfovo, *Phys. Rev. Lett.* **90**, 060404 (2003).
 - ⁶⁶ L.-M. Duan, *Phys. Rev. Lett.* **96**, 103201 (2006).